

***TFEB* Amplification Renal Cell Carcinoma Detected by Chromosome Genomic Array Testing: A Case Report for Diagnosis of a Novel Entity**

Xiaoyu Qu^{1,7*}, Maria S. Tretiakova^{2*}, Yingbei Chen³, John A. Thompson^{1,4}, Daniel Lin^{1,5}, Ramasamy Bakthavatsalam^{5,6}, Cristina R. Antonescu³, Scott S. Tykodi^{1,4} and Min Fang^{1,2,7}

¹Clinical Research Division, Fred Hutchinson Cancer Research Center, 1100 Fairview Ave. N., Seattle, WA 98109

²Department of Pathology, University of Washington, 1959 NE Pacific St., Seattle, WA 98195

³Department of Pathology, Memorial Sloan Kettering Cancer Center, 1275 York Avenue, New York, NY 10065

⁴Department of Medicine, Division of Medical Oncology, University of Washington, 1959 NE Pacific St., Seattle, WA 98195

⁵Department of Urology, University of Washington, 1959 NE Pacific St., Seattle, WA 98195

⁶Department of Surgery, University of Washington, 1959 NE Pacific St., Seattle, WA 98195

⁷Clinical Cytogenetics, Seattle Cancer Care Alliance, 825 Eastlake Ave. E., Seattle, WA 98109

*Corresponding author: Min Fang, M.D., Ph.D., FACMG, Fred Hutchinson Cancer Research Center 825 Eastlake Ave. E., G7-500, Seattle, WA 98109-1023, Tel: (206) 288-1385; E-mail: mfang@fhcrc.org

Received date: January 10, 2017; Accepted date: February 09, 2017; Published date: February 18, 2017

Citation: Qu X, Tretiakova MS, Chen Y, Thompson JA, Lin D, et al. (2017) *TFEB* amplification renal cell carcinoma detected by chromosome genomic array testing: A case report for diagnosis of a novel entity. J Clin Mol Pathol 1: 07.

Copyright: © 2017 Qu X et al. This is an open-access article distributed under the terms of the Creative Commons Attribution License, which permits unrestricted use, distribution, and reproduction in any medium, provided the original author and source are credited.

Abstract

Background: The accurate diagnosis and corresponding prognosis of renal cell carcinoma (RCC) are challenged by overlapping histological features and imprecise immunohistochemical (IHC) markers, which easily leads to misdiagnosis of rare subtypes, such as translocation RCC (tRCC).

Case presentation: We report here a rare case of *TFEB* amplified RCC presenting in a 47-year-old male with a 10 cm renal mass and regional lymph node metastases. This tumor was initially diagnosed as a clear cell RCC (ccRCC). However, chromosome genomic array testing (CGAT) revealed *TFEB* gene amplification, which was confirmed by fluorescent in situ hybridization (FISH). *TFEB* transcript overexpression was demonstrated by RNA in situ hybridization. The tumor histology was reassessed and relabelled as unclassified RCC based on unusual histologic features and a non-specific IHC profile. The tumor rapidly progressed with distant metastatic disease that responded to treatment with sunitinib for 11 months.

Conclusions: *TFEB* gene amplification without rearrangement/translocation appears to be a novel entity. Ours is a rare *TFEB* gene amplification RCC case with metastasis and unusual morphology. The workup of our case demonstrates the potential role for CGAT to aid in the subtype classification of RCC tumors.

Keywords: Amplification; CGAT/CGH; Metastasis; RCC; *TFEB*; Case Report

Background

MiTF family translocation renal cell carcinoma (tRCC) is a subtype of renal cell carcinoma (RCC) harbouring translocations involving the microphthalmia transcription factors (MiTF) family members: [1] transcription factor for immunoglobulin heavy-chain enhancer 3 (*TFE3*) located on the short arm of chromosome X (Xp11.2); and less commonly [2] the T-cell transcription factor EB (*TFEB*) located on the short arm of chromosome 6 (6p21). At the molecular level, *TFE3* has multiple rearrangement partners [1], whereas *TFEB* is primarily fused with metastasis associated lung adenocarcinoma transcript 1 (*MALAT1*, 11q12) [2] although additional novel partners have been recently discovered [3,4]. These rearrangements lead to overexpression of the corresponding *TFE3* and *TFEB* proteins, which can be detected by immunohistochemistry (IHC) to facilitate the diagnosis of these rare tumors, although IHC for *TFE3* and *TFEB* proteins has much lower sensitivity and specificity compared to FISH [5-7].

Distinct from the common histologic subtypes of RCC, *TFE3* tRCCs occur in younger patients, representing one-third of pediatric RCC tumors and up to 15% of RCC presenting below the age of 45, have a female predominance [8], and are frequently associated with an aggressive clinical course. Collected series of *TFEB* tRCC similarly present at a young age, but typically demonstrate an indolent clinical course with a few exceptions [9-11].

The two types of tRCCs have some unique morphologic features; however, histological assessment alone is not sufficient for the diagnosis of tRCC, as it often resembles other subtypes of renal carcinomas, most commonly clear cell RCC and papillary RCC [6,7]. A recent study using The Cancer Genome Atlas (TCGA)

dataset identified 1.5% of the RCC cases that were initially classified as clear cell were in fact tRCC [12]. Moreover, comprehensive molecular analysis of papillary RCCs from TCGA dataset identified 8 out of 161 tumors with *TFE3* or *TFEB* gene fusions [4]. A diagnosis of tRCC is confirmed by the presence of chromosomal translocation and/or strong and diffuse nuclear expression of TFE proteins in tumor cells. Although these criteria seem relatively straight forward, their application can be technically challenging and is variable among different institutions. According to a recent member survey by the International Society of Urological Pathology (ISUP), the current consensus is that *TFE3* and *TFEB* analysis should be requested when RCC is diagnosed in a young patient or when the histologic appearance suggests the translocation subtype [7]. However, there is no consensus at present regarding whether fluorescent in situ hybridization (FISH) or IHC should be performed [7]. In addition, IHC for *TFEB* is often equivocal, difficult to perform and interpret, and is available only at a few academic laboratories.

Chromosome Genomic Array Test (CGAT) is now used clinically for the assessment of multiple cancer types. This whole-genome approach provides comprehensive evaluation of the entire cancer genome for copy number alterations and loss of heterozygosity, which cannot be achieved by FISH or IHC. The high resolution of CGAT enables detection of submicroscopic aberrations undetectable by conventional cytogenetics. Here, we present the detailed molecular, morphologic and clinical characterization of an aggressive RCC tumor with *TFEB* gene amplification that was detected by CGAT and confirmed by FISH and RNA in situ hybridization (RNA ISH).

Case Presentation

Clinical presentation of the patient

The patient, a 47-year-old male, sought medical attention because of gross hematuria and right flank pain. Computerized tomography (CT) and magnetic resonance imaging (MRI) revealed a large right renal mass invading the renal hilum and measuring 8.9 x 6.5 cm. Additional findings included retroperitoneal lymphadenopathy up to 2.0 cm, and tumor thrombus within the right renal vein extending into the inferior vena cava (IVC) up to the dome of the liver. The patient underwent a right radical nephrectomy, with IVC mobilization and thrombectomy along with a retroperitoneal lymph node dissection.

Gross findings

The tumor was located in the upper and middle parts of the right kidney and measured 10 x 8 x 7 cm. On cut section, the tumor was variegated, tan-brown in color with areas of hemorrhage and necrosis, and had a multinodular appearance. The dominant bulging nodule penetrated through the renal

capsule. Multiple smaller satellite nodules were revealed in the renal hilum, calyces and perinephric fat (Figure 1A and 1B). The right renal vein contained a 2.4 cm tumor thrombus. Two matted retrocaval lymph nodes and one matted enlarged inter-aortocaval lymph node contained focally necrotic metastatic tumor deposits measuring up to 4.5 cm in greatest dimension. The right adrenal gland was present and unremarkable.

Histologic findings

The presence of RCC was confirmed in the tumor thrombus. Non-neoplastic renal parenchyma was hemorrhagic and ischemic. Metastases were detected in three out of the three regional matted lymph nodes, which were completely replaced by the tumor with multifocal extracapsular extension. Additionally, tumor extension was noted within hilar fat along calyces and proximal ureter with invasion into the muscularis propria (Figure 1C).

The tumor histology was originally determined to be consistent with clear cell renal cell carcinoma (ccRCC), Fuhrman grade 3 (ISUP grade 3). On further detailed histologic examination, the tumor architecture was characterized as variable and composed of large areas with papillary, tubular and solid architecture, and smaller compact nests and acini demarcated by variable in thickness fibrovascular septae (Figures 2A and 2D). The majority of tumor cells were large, polygonal, with predominantly eosinophilic cytoplasm and high-grade nuclei with prominent nucleoli. Due to the presence of large bizarre nuclei and gigantic nucleoli visible at low power (40x), the tumor was upgraded from original Fuhrman grade 3 to grade 4 (ISUP grade 4). The quality of cytoplasmic content ranged from pale with focal clearing to finely granular to coarsely granular oncocyctic look with intracytoplasmic inclusions. Additionally, there were also numerous smaller plasmacytoid and histiocytic cells demonstrating densely bright eosinophilic cytoplasm, lower grade nuclei, and mild to moderate nuclear pleomorphism. These abundant smaller cells were clustered together filling spaces within acini, tubules and between papillary structures formed by the larger polygonal cells. Mitoses were present in both larger and smaller cells, and quite abundant, reaching up to 5 mitotic figures per high power field including occasional pathologic forms (Figures 2E and 2F). Necrosis was present and comprised around 10% of tumor volume histologically. Tumor morphologies within kidney, lymph node metastases and venous thrombus were identical displaying biphasic morphology of intimately admixed populations of large eosinophilic polygonal cells and sheets of smaller plasmacytoid and histiocytic cells. We also noted modest amounts of tumor infiltrating lymphocytes and plasma cells within fibrovascular cores and fibrotic septae. Despite active searching, small rounded nodules of hyaline, basement membrane-like material, characteristically described in non-aggressive *TFEB* tumors, were not detected.

Figure 1

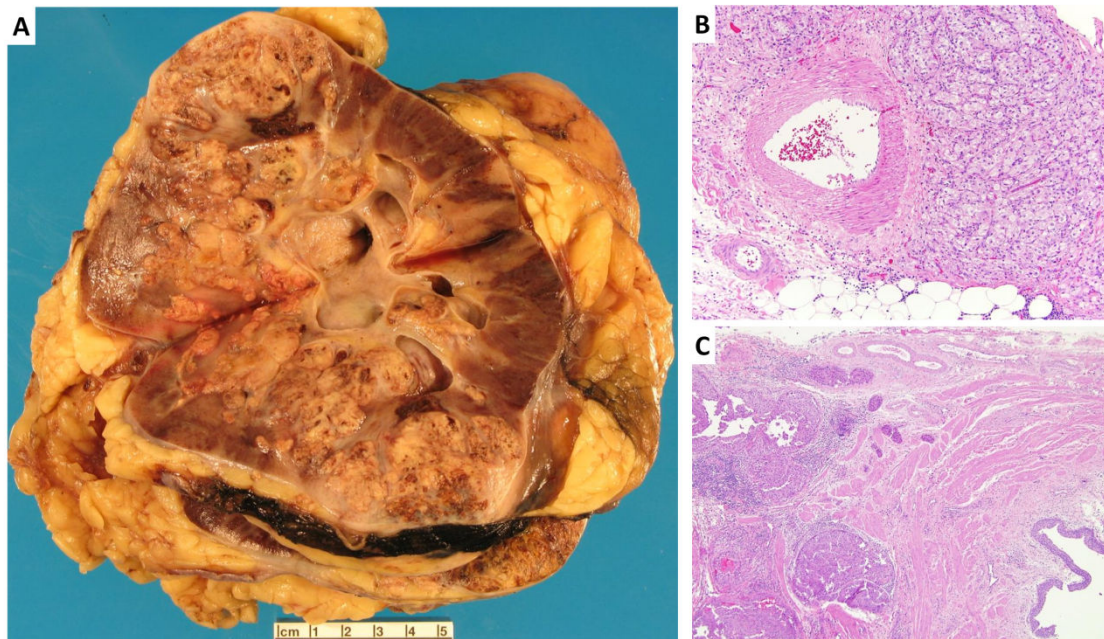


Figure 1: Gross photograph of kidney mass (A) with apparent aggressive features, including large size (10 x 8 x 7 cm), multinodular growth pattern, variegated cut surface with areas of hemorrhage and necrosis, and infiltrative borders with penetration of the kidney capsule. There is multifocal invasion of sinus and perinephric fat (B), gross extension into the renal vein, multiple metastases within regional lymph nodes and invasion of proximal ureter muscle wall (C).

Figure 2

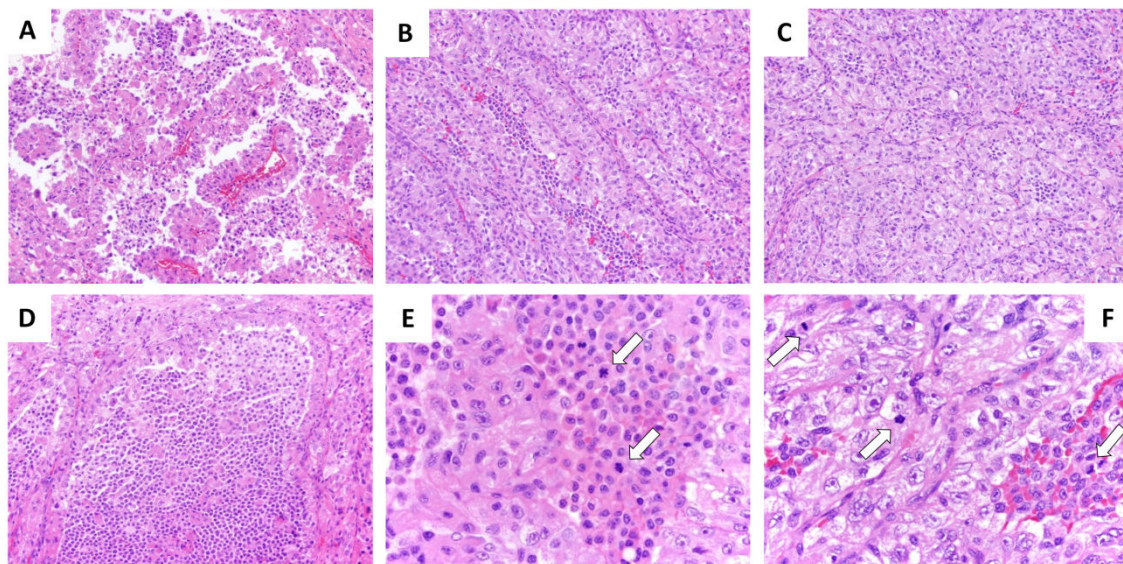


Figure 2: Representative images of *TFEB* amplification tumor showing biphasic morphology displaying discohesive papillary (A), tubular (B), compact acinar (C) architecture, and solid sheets of smaller cells confined within expanded tubules (D). All architectural patterns contain two intimately admixed cell populations consisting of large polygonal eosinophilic cells with high-grade nuclei and smaller plasmacytoid or slightly elongated histiocytic cells. At higher magnification, both cell populations are mitotically active (E-F, arrows). Original magnification 100x (A-D) and 200x (E-F).

Immunohistochemical (IHC) phenotype

The immunohistochemical findings are summarized in Table 1 and Figure 3. The staining patterns were different across the two cell populations. The large eosinophilic polygonal cells were strongly highlighted by PAX8 and CAM5.2, supporting their renal epithelial origin, whereas small cells preferentially expressed Vimentin, CD68 and CD163 confirming their histiocytic origin. Proliferation marker Ki-67 was expressed in both large and small cell populations with the proliferation index reaching up to 20% of nuclei. In addition, larger cells also strongly expressed CD138 (plasma cell marker), which was negative in smaller plasmacytoid cells. Cathepsin-K and epithelial membranous antigen (EMA) immunostaining were focally positive in rare

scattered larger tumor cells, whereas CAIX was variably positive in both large and small cells, especially in areas adjacent to tumor necrosis. CK7, CKIT, melanoma markers HMB45 and Melan A, as well as *TFE3*, were all negative in both large and small tumor cells, however CK7 and EMA highlighted an infiltrative tumor growth pattern by staining entrapped benign renal structures. Strong CD45 staining of tumor infiltrating lymphocytes was present highlighting their small amounts compared to the abundant atypical histiocytic cell population which was weakly and focally positive for CD45. There was no significant difference in the immunoprofile between primary and metastatic tumor nodules.

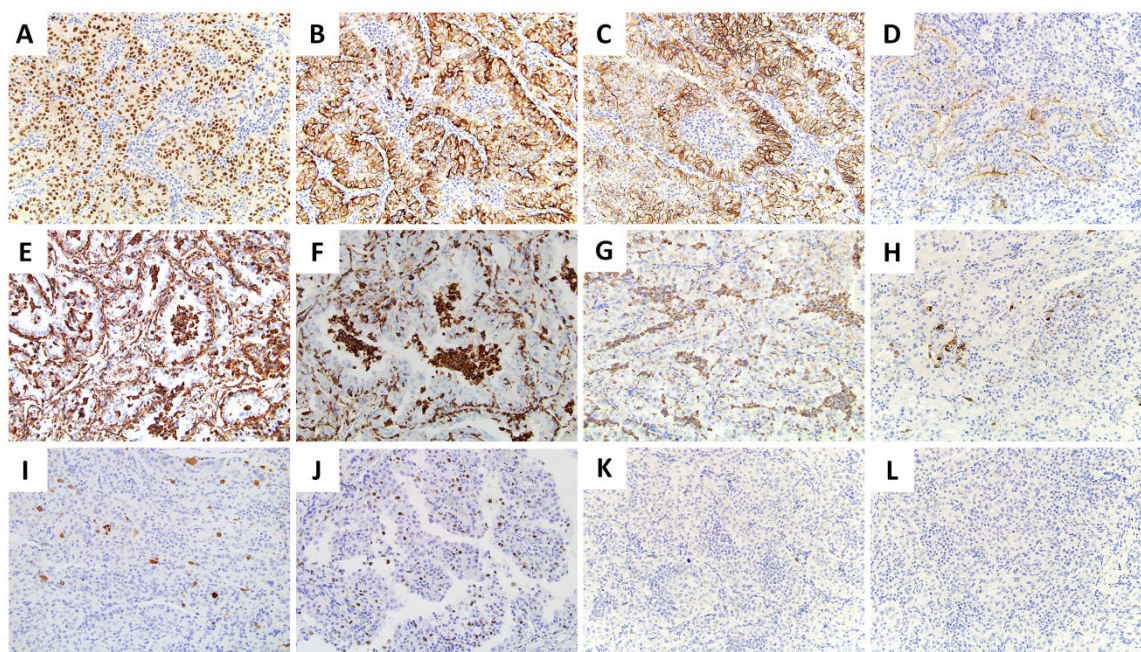


Figure 3: Immunostaining of *TFEB* amplification tumor with biphasic morphology shows preferential expression of markers PAX8 (A), CAM5.2 (B), CD138 (C) and CD10 (D) in the larger epithelial cells, whereas Vimentin (E), CD163 (F) and CD68 (G) highlight only smaller cells of histiocytic nature. There is also scattered positivity of the large epithelial cells with EMA (H) and Cathepsin K (I). Cathepsin K also noted in small inflammatory cells. Ki67 showed proliferation rates 10-20% (J). Tumor cells are negative for, CKIT (K), melanocytic markers Melan A (L) and HMB45, as well as CK7 and *TFE3* (not shown). All pictures are taken at magnification 200x.

Molecular cytogenetic findings

CGAT revealed a 14-Mb segment with copy number gain located on the short arm of chromosome 6 (Figure 4). The peak region of the gain was estimated to be five to six copies, encompassing the *TFEB* and cyclin D3 (*CCND3*) gene loci. In addition, numerous copy number aberrations were seen including high-level gains of 6p12 and 8p11, as well as low-level gains of 1q, 3q, 4p, 6q, and 8q and deletions of 1p, 2q, 3p, 6p, 8p, 11q, 13, 14, 16q, 17p, 18q, and 22q (Figure 4A). Among these low-level abnormalities, 3p deletion is considered a hallmark of ccRCC. FISH showed *TFEB* gene amplification without evidence of *TFEB* rearrangement (Figures 5A and 5B). There were variable numbers of *TFEB* probe signals per nucleus. QuantiGene ViewRNA ISH also showed areas with high levels of

TFEB RNA (Figure 5C) as well as regions with low to no expression (Figure 5D) while controls performed appropriately.

Disease course and response to therapy

Post-operative CT imaging identified multiple new pulmonary nodules and enlarging retroperitoneal lymphadenopathy consistent with metastatic disease. The patient received systemic therapy with high dose interleukin-2 (IL2) without response followed by sunitinib, an oral multi-kinase inhibitor. He had an excellent initial response to sunitinib, but after 11 months progressed. He then switched to everolimus, a mammalian target of rapamycin (mTOR)-inhibitor, but had no response. The patient then was treated with bevacizumab (a monoclonal antibody targeting the vascular endothelial growth

factor) plus interferon, but did not tolerate interferon which was discontinued. As of the last follow up at 2 years post-surgery, the patient was continuing on bevacizumab. Restaging CT imaging revealed bulky mediastinal lymphadenopathy, innumerable

bilateral pulmonary nodules, multiple new lesions in the retroperitoneum, new nodules in the left adrenal gland and an osteolytic focus in the L1 vertebra.

Table 1: Detailed immunohistochemical results of aggressive *TFEB* amplification RCC.

Antibody	Vendor	Clone	Dilution	Staining pattern	Localization of expression	Figure
PAX8	Cell Marque	MRQ-50	1:100	+++ , diffuse	Large cells only	3A
CAM5.2	BD	CK8	1:50	+++ , diffuse	Large cells only	3B
CD138	Biocare	B-A38	1:100	++ , diffuse	Large cells only	3C
CD10	Novocastra	CD10	1:100	+ , focal	Large cells only	3D
Ki67	DAKO	MIB1	1:200	10-20%	Large and small cells	3J
Vimentin	DAKO	M76	1:2000	+++ , diffuse	Small cells only	3E
CD68	Cell Marque	KP1	1:4000	++ , diffuse	Small cells only	3G
CD163	Novocastra	10DG	1:100	+++ , diffuse	Small cells only	3F
CAIX	Novocastra	TH22	1:100	+ , multifocal	Predominantly small cells	
EMA	DAKO	E29	1:1000	+ , focal	Rare positive large cells	3H
Catepsin K	Abcam	3F9	1:800	+ , focal	Rare positive large cells	3I
CD45	DAKO	2B11+PD7/26	1:100	+/-	Lymphocytes (strong) and small cells (weak)	
CK7	DAKO	OV-TL	1:500	-	Entrapped tubules	
CKIT	DAKO	polyclonal	1:500	-	Mast cells only	3K
HMB45	Novocastra	HMB45	1:400	-	-	
Melan A	DAKO	A103	1:200	-	-	3L
TFE3	Santa Cruz	polyclonal	1:100	-	-	

Methods

Immunohistochemistry (IHC)

IHC was performed on FFPE sections using an automated immunostainer [Bond III (TM), Leica Biosystems, Germany] and a standardized protocol as previously described [14].

For antigen retrieval either ER1 (pH=8) or ER2 (pH=9) proprietary buffers were applied for 20 min. Following several rinses and endogenous peroxidase blocking step, a post primary IgG linker was applied. Then the slides were incubated with either rabbit polyclonal or mouse monoclonal antibodies for 15 min (Table 1). Following multiple rinses with proprietary Bond Wash solution (Leica Biosystems, Germany), a Poly-HRP-IgG polymer solution was applied (either anti-mouse or anti-rabbit). This step was followed by 8 min incubation with polymer detection reagent, after which the slides were rinsed, incubated with 3,3'-Diaminobenzidine tetrahydrochloride chromogen, and hematoxylin counterstained.

Chromosome Genomic Array Test (CGAT) with OncoScan™

Genomic DNA was isolated from a formalin-fixed-paraffin-embedded (FFPE) tissue specimen using the QIAamp DSP DNA FFPE Tissue Kit (Qiagen, Valencia, CA). CGAT was performed using the OncoScan™ FFPE assay kit (Affymetrix, Santa Clara, CA), which contains 220,000 single-nucleotide polymorphism (SNP) probes and is specifically designed to provide high coverage/resolution for determining copy number aberrations (CNAs) and loss of heterozygosity (LOH) in genomic regions encompassing cancer genes. Samples were processed according to the manufacturer's recommendation. OSCHP files were generated using the OncoScan™ Console (OC) Software (Affymetrix) and visualized with Nexus Expression OncoScan software (BioDiscovery, Elsecondo, CA) and Chromosome Analysis Suite (ChAS, Affymetrix).

Figure 4

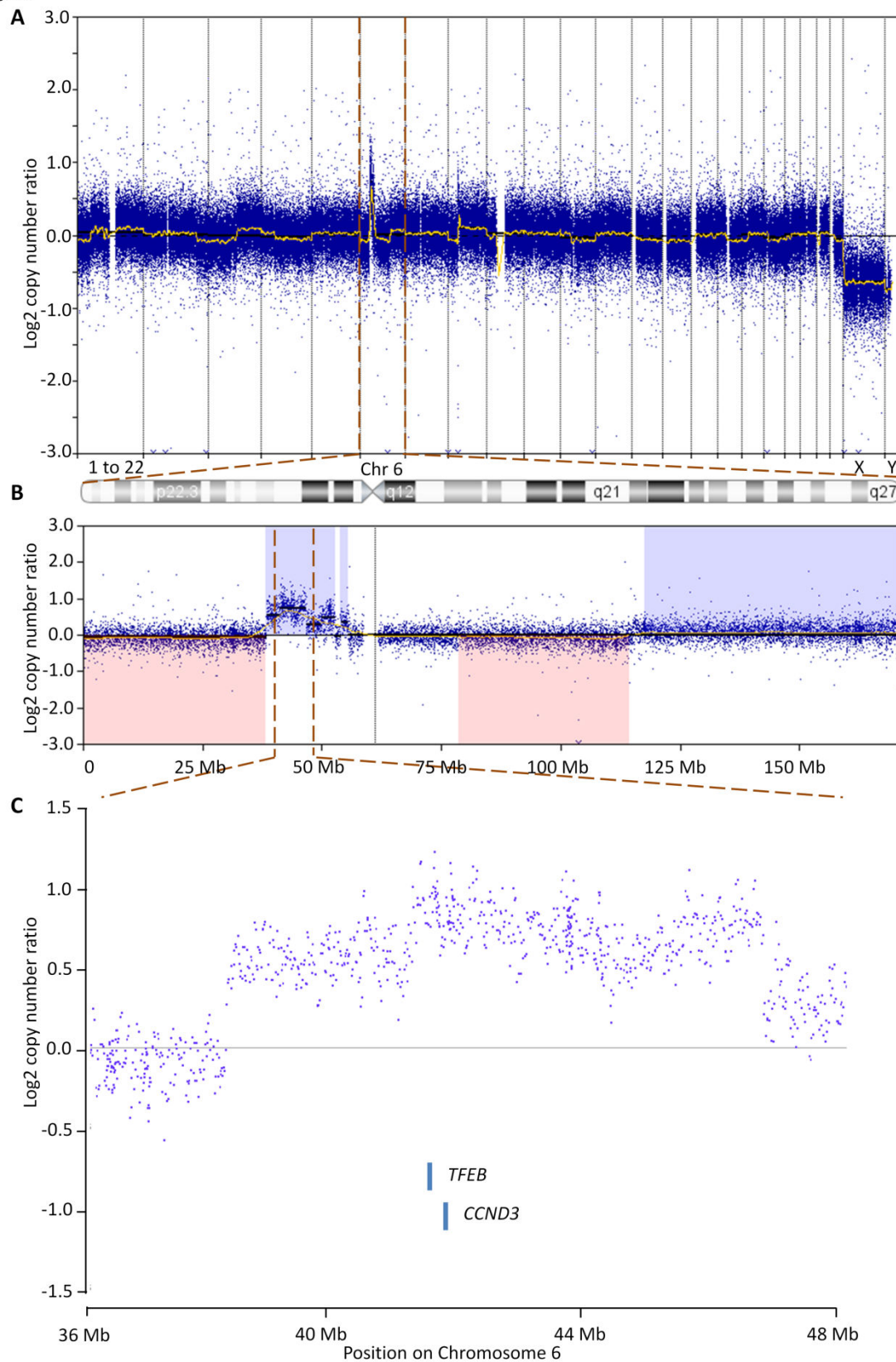


Figure 4: Chromosome genomic array testing (CGAT) detected *TFEB* amplification. (A) The whole genome plot view demonstrating copy number aberrations (CNAs) of the sample; (B) CNAs on chromosome 6; and (C) The region encompassing the *TFEB* locus on the short arm of chromosome 6. Each blue dot corresponds to a probe on the array. The X axis denotes genomic location, while the Y axis denotes log₂ ratio of the copy number. In (A) and (B), the yellow line depicts a moving average value. In (B), pink and blue shades denote deletions and gains, respectively.

Figure 5

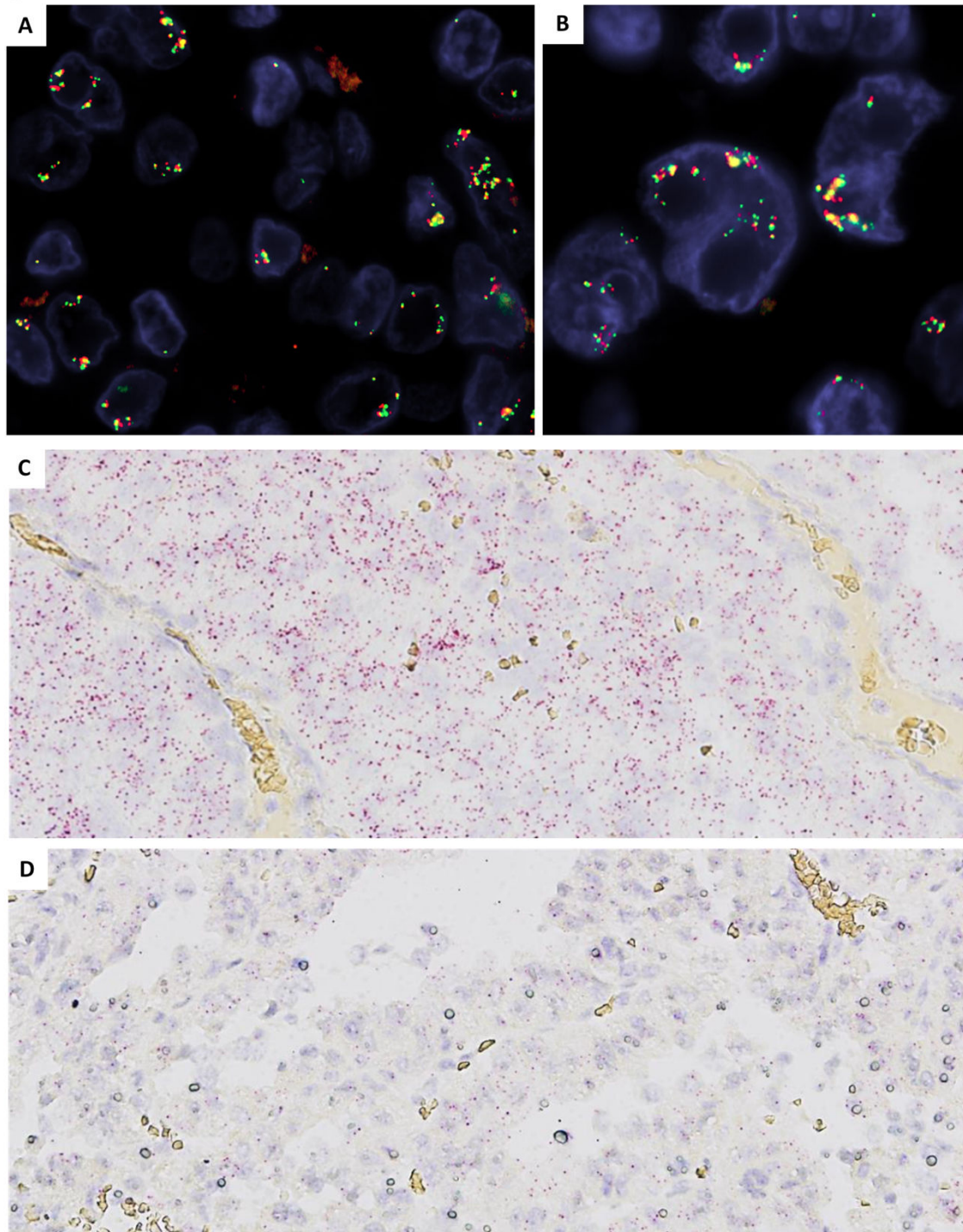


Figure 5: *TFEB* amplification detected by both DNA and RNA in situ hybridization. (A) Low-power view of DNA FISH results showing uniform pattern of co-amplification of centromeric (red) and telomeric (green) signals of *TFEB* gene. (B) High-power view of DNA FISH showing numerous (>10 copies) *TFEB* gene as indicated by multiple red, green and overlapping yellow fluorochrome signals. (C) and (D) Bright-field view (20x) of RNA ISH demonstrating areas with high (C) and low (D) levels of *TFEB* RNA expression.

CNAs greater than 500 Kb in size and copy-neutral LOH greater than 10 Mb are considered abnormal based on the established performance characteristics of the assay validated in our CLIA-certified diagnostic laboratory.

Fluorescence in Situ Hybridization (FISH)

FISH on interphase nuclei was performed as previously described [15] on 4 micron thick FFPE sections with custom break-apart probes covering the *TFEB* locus at 6p21.1. Bacterial

artificial chromosomes (BAC) clones were selected and acquired from the Children's Hospital of Oakland Research Institute (CHORI) (Oakland, CA) (<http://bacpac.chori.org>). After DNA extraction from individual BACs, different fluorochromes were used to label them in a nick translation reaction: BACs located near the 5' of *TFEB*, RP11-1084M7 and RP11-7K24, were labeled red (552 dUTP, Enzo Life Sciences, Farmingdale, NY), while the BACs located near the 3' of the gene, RP11-81C24 and RP11-185M21, were labeled green (Green 496 dUTP, Enzo Life Sciences). This step was followed by FISH probes denaturing, hybridization to pretreated slides, incubation, multiple washes and mounting with DAPI in an anti-fade solution. The signals were visualized and counted on 200 successive nuclei using a fluorescence microscope (Zeiss Axioplan, Oberkochen, Germany), controlled by Isis 5 software (Metasystems; Watertown, MA). At least 20% nuclei with signal were required for positive score where amplification was defined as a ratio equal or greater than 10:1 of *TFEB* signal in tumor cells to reference normal cells.

QuantiGene viewRNA ISH

The in situ hybridization for *TFEB* RNA was performed at Affymetrix on the FFPE tissue slide using the QuantiGene ViewRNA ISH Tissue Assay Kit (Affymetrix, Santa Clara, CA). The sample was carried through pretreatment boiling for 10 min and protease incubation for 20 min prior to hybridization using a *TFEB* probe. The target RNA was detected using a Fast Red Substrate, which was visualized using a standard bright field microscope.

Discussion

Herein we report the rare finding of *TFEB* amplification in an RCC tumor and describe the associated genomic findings, pathological phenotype and clinical behavior. Currently, *TFEB* gene rearrangement via a translocation between chromosomes 6 and 11 [t(6; 11)(p21;q12)] is thought to be the primary mechanism leading to the dysregulation of *TFEB* by promoter substitution resulting in oncogene overexpression in *TFEB* tRCC [10].

Most reported RCC cases with *TFEB* gene amplification showed concurrent *TFEB* rearrangement. The first case that presented as metastatic tRCC in a female patient was reported by Peckova et al. [11]. *TFEB* amplification in this tumor was demonstrated by FISH, along with *Alpha-TFEB* rearrangement [t(6;11)(p21;q12)] confirmed by reverse transcription polymerase chain reaction (RT-PCR). This was a female patient, who was diagnosed at age 77 with a 12 × 11.5 × 9 cm tumor with 40% necrosis and adrenal gland and lung metastasis, and died at 2.5 months after diagnosis. The second case reported by Durinck et al. [3] was detected by CGAT that showed an amplified segment on chromosome 6 encompassing *TFEB* and *CCND3*, similar to our case. *TFEB* amplification was confirmed by FISH. In addition, this tumor also had segmental amplification within chromosome 7 encompassing *MET*, but no change in the expression of key genes involved in *MET* signaling and metabolism was found. The clinical outcome was not discussed in the report, but the tumor was initially classified as papillary

RCC (pRCC). The authors described it as low-grade RCC with papillary and oncocytic features. A combination of papillary and oncocytic features is characteristic of pRCC, type 2, which is the more aggressive papillary RCC subtype. Recent comprehensive genomic analysis of 161 papillary RCCs (TCGA dataset) showed two cases with high mRNA expression of the *TFEB* transcript and also the more aggressive type 2 tumors; but neither showed *TFEB* gene amplification. In both cases, the high mRNA expression was due to *TFEB* fusions involving novel fusion partners *COL21A1* and *CADM2* [4].

CGAT on our case revealed a complex abnormal genome that included deletion of the short arm of chromosome 3 present at a very low level. However, the dominant abnormality (i.e., the main clone) was the segmental amplification on chromosome 6 that encompassed *TFEB*, a finding that was verified by FISH. *TFEB* overexpression was subsequently demonstrated by RNA ISH. Intra-tumor heterogeneity was evident that *TFEB* amplified/overexpressed cells appeared to be the larger cells. Our patient had an aggressive disease course progressing to metastatic disease shortly after nephrectomy surgery. The aggressive clinical course and poor outcome for at least two of these three patients with tRCC harboring *TFEB* amplifications is noteworthy as *TFEB* tRCC are typically recognized as indolent tumors [10,11,16]. Only a few *TFEB*-positive cases with metastases have been reported to date, recently summarized by Peckova et al. [11]. These tumors were diagnosed as *TFEB* translocated RCC by various methodologies, including one with IHC alone [17], one with IHC, G-banding cytogenetics, and polymerase chain reaction (PCR)-based methods [18], and two with FISH [11,19]. Due to the limitations of these different techniques, it is uncertain if undetected gene amplification was present in some of these tumors. Further analysis of these and/or additional tRCC tumors will be instructive to determine if *TFEB* amplification may differ from *TFEB* rearrangement in their prognosis.

Initially, our case was classified histologically as ccRCC. On further analysis, this patient's tumor showed variable papillary, solid and nested architecture, biphasic morphology coupled with an aggressive infiltrative growth pattern, high-grade nuclear features in the majority of cells, presence of large bizarre cells consistent with Fuhrman grade 4 (ISUP grade 4), high mitotic activity confirmed by the Ki67 proliferation marker and tumor necrosis. Two intimately admixed cell populations had peculiar immunohistochemical profiles not seen in any known variant of renal cell carcinoma. The larger cell population was consistent with a renal epithelial origin. These cells also showed scattered reactivity with Cathepsin K (surrogate marker of translocation RCC) [9]. The smaller cell population expressed markers supporting its histiocytic origin with strong reactivity for CD163 and Vimentin. Interestingly, in a recent study Behnes, et al. [20] reported that papillary RCC type 2 not only frequently had abundant tumor-associated macrophages (TAM), but nearly all of them expressed CD163, a characteristic marker for M2 macrophages. The immunosuppressive M2 phenotype of TAMs, which are strongly positive for CD163 as in our case, is associated with increased tumor growth, invasiveness and metastasis. Thus our case also shares similarities with papillary RCC, type 2, including the presence of a subpopulation of

actively proliferating CD163 positive macrophages, multifocal papillary architecture, high nuclear grade, cellular pseudostratification and oncocytic phenotype of malignant epithelial cells.

The identification of the *TFEB* gene amplification in this case highlighted the effective clinical utility of chromosomal genomic array testing (CGAT) in the diagnostic workup of RCC. RCC classification based on histologic evaluation is prone to misdiagnosis due to overlapping histopathological features of different tumor types and the numerous possibilities in choosing targeted reflex assays. This is especially challenging for the diagnosis and prognosis of the rare tumor types. CGAT characterization of whole-genome CNAs in RCC can assist with histological classification as well as prognostic risk stratification among clear cell tumors [21]. Conventional cytogenetic characterization of RCC is labor intensive with a high failure rate because of challenges with culturing RCC cells in vitro and is wholly dependent on a source of viable tumor tissue. In contrast, CGAT with OncoScan™ allows for a consistent, high-resolution, and robust workup of RCC specimens that is suitable for analysis of archival FFPE tissues.

Optimal systemic treatment for advanced *TFEB* tRCC has not been defined. The incidence of tRCC in a young patient population encourages the consideration of high dose IL-2 for select patients. However, favorable outcomes of *TFE3* tRCC tumors treated with cytokine immunotherapies have not been seen in small case series [22]. Our patient had no response to IL-2, but had a period of disease control with antiangiogenic therapy with sunitinib. The overall treatment course for our patient was comparable to outcomes that have been described for *TFE3* tRCC patients [22].

In summary, we present here a rare *TFEB* amplified RCC case with metastasis and unusual morphology with dual epithelial and histiocytic cell populations. The workup of our case demonstrated that, with proper design, CGAT can identify multiple genomic lesions in one test with a fast turn-around time (a few days). This is especially useful in the evaluation of solid tumors that [1] have highly heterogeneous cytogenomic profiles [12] and therefore cannot be effectively assessed using targeted analyses alone such as IHC and FISH; and [2] have similar IHC finding but may differ significantly in disease outcomes depending on the underlying genomic mechanisms. More such cases are being identified with the wider use of CGAT in clinical workup of RCC patients; as a result, *TFEB* gene amplification without rearrangement/translocation appears to be a novel entity. At the time of review of this report, Argani et al. published additional cases of *TFEB*-amplified RCC specifically with variable melanocytic marker expression, supporting the notion of a novel entity [23].

Ethics Approval

The IRB at Fred Hutchinson Cancer Research Center provided ethics approval for the research conducted for this manuscript.

Competing Interests

The authors declare that they have no financial or non-financial competing interests.

Funding

There are no funding sources for the research reported; only departmental funding was utilized.

Authors' Contributions

XQ, MST, SST and MF contributed to the conception and design of the study. XQ, MST, YC, JT, DL, RB, CRA, SST and MF contributed to the provision of study material, patient recruitment, and acquisition of data. XQ, MST and MF collected and assembled the data. XQ, MST, SST and MF participated in drafting of the manuscript. All authors revised the manuscript critically, and gave final approval to submit for publication.

Acknowledgements

We thank Scott McElhone from the Seattle Cancer Care Alliance for technical assistance with the OncoScan analysis. We thank Mr. Wilson Lew and Dr. Eric Fung from Affymetrix Inc for performing the RNA ISH assay.

References

1. Malouf GG, Camparo P, Molinie V, Dedet G, Oudard S, et al. (2011) Transcription factor E3 and transcription factor EB renal cell carcinomas: clinical features, biological behavior and prognostic factors. *J Urol.* 185: 24-29.
2. Argani P, Lae M, Hutchinson B, Reuter VE, Collins MH, et al. (2005) Renal carcinomas with the t(6;11)(p21;q12): clinicopathologic features and demonstration of the specific alpha-TFEB gene fusion by immunohistochemistry, RT-PCR, and DNA PCR. *Am J Surg Pathol.* 29: 230-240.
3. Durinck S, Stawiski EW, Pavia-Jimenez A, Modrusan Z, Kapur P, et al. (2015) Spectrum of diverse genomic alterations define non-clear cell renal carcinoma subtypes. *Nature genetics* 47: 13-21.
4. Cancer Genome Atlas Research N (2016) Comprehensive Molecular Characterization of Papillary Renal-Cell Carcinoma. *N Engl J Med.* 374: 135-145.
5. Hayes M, Peckova K, Martinek P, Hora M, Kalusova K, et al. (2015) Molecular-genetic analysis is essential for accurate classification of renal carcinoma resembling Xp11.2 translocation carcinoma. *Virchows Arch.* 466: 313-322.
6. Magers MJ, Udager AM, Mehra R (2015) MiT Family Translocation-Associated Renal Cell Carcinoma: A Contemporary Update With Emphasis on Morphologic, Immunophenotypic, and Molecular Mimics. *Arch Pathol Lab Med.* 139: 1224-1233.
7. Tan PH, Cheng L, Rioux-Leclercq N, Merino MJ, Netto G, et al. (2013) Renal tumors: diagnostic and prognostic biomarkers. *Am J Surg Pathol.* 37: 1518-1531.
8. Argani P, Olgac S, Tickoo SK, Goldfischer M, Moch H, et al. (2007) Xp11 translocation renal cell carcinoma in adults: expanded clinical, pathologic, and genetic spectrum. *Am J Surg Pathol.* 31: 1149-1160.

9. Argani P (2015) MiT family translocation renal cell carcinoma. *Semin Diagn Pathol.* 32: 103-113.
10. Kauffman EC, Ricketts CJ, Rais-Bahrami S, Yang Y, Merino MJ, et al. (2014) Molecular genetics and cellular features of TFE3 and TFEB fusion kidney cancers. *Nat Rev Urol.* 11: 465-475.
11. Peckova K, Vanecek T, Martinek P, Spagnolo D, Kuroda N, et al. (2014) Aggressive and nonaggressive translocation t(6;11) renal cell carcinoma: comparative study of 6 cases and review of the literature. *Ann Diagn Pathol.* 18: 351-357.
12. Malouf GG, Monzon FA, Couturier J, Molinié V, Escudier B, et al. (2013) Genomic heterogeneity of translocation renal cell carcinoma. *Clinical cancer research : an official journal of the American Association for Cancer Research.* 19: 4673-4684.
13. Rao Q, Williamson SR, Zhang S, Eble JN, Grignon DJ, et al. (2013) TFE3 break-apart FISH has a higher sensitivity for Xp11.2 translocation-associated renal cell carcinoma compared with TFE3 or cathepsin K immunohistochemical staining alone: expanding the morphologic spectrum. *Am J Surg Pathol* 37: 804-815.
14. Andeen NK, Tretiakova MS (2016) Metastatic Treated Malignant Germ Cell Tumors: Is SALL4 a Better Marker Than Placental Alkaline Phosphatase? *Appl Immunohistochem Mol Morphol.* 24: 210-214.
15. Antonescu CR, Zhang L, Shao SY, Mosquera JM, Weinreb I, et al. (2013) Frequent PLAG1 gene rearrangements in skin and soft tissue myoepithelioma with ductal differentiation. *Genes Chromosomes Cancer* 52: 675-682.
16. Rao Q, Liu B, Cheng L, Zhu Y, Shi QL, et al. (2012) Renal cell carcinomas with t(6;11)(p21;q12): A clinicopathologic study emphasizing unusual morphology, novel alpha-TFEB gene fusion point, immunobiomarkers, and ultrastructural features, as well as detection of the gene fusion by fluorescence in situ hybridization. *Am J Surg Pathol.* 36: 1327-1338.
17. Camparo P, Vasiliu V, Molinie V, Couturier J, Dykema KJ, et al. (2008) Renal translocation carcinomas: clinicopathologic, immunohistochemical, and gene expression profiling analysis of 31 cases with a review of the literature. *Am J Surg Pathol.* 32: 656-670.
18. Inamura K, Fujiwara M, Togashi Y, Nomura K, Mukai H, et al. (2012) Diverse fusion patterns and heterogeneous clinicopathologic features of renal cell carcinoma with t(6;11) translocation. *Am J Surg Pathol.* 36: 35-42.
19. Smith NE, Illei PB, Allaf M, Gonzalez N, Morris K, et al. (2014) t(6;11) Renal Cell Carcinoma (RCC): expanded immunohistochemical profile emphasizing novel RCC markers and report of 10 new genetically confirmed cases. *Am J Surg Pathol.* 38: 604-614.
20. Behnes CL, Bremmer F, Hemmerlein B, Strauss A, Strobel P, et al. (2014) Radzun HJ. Tumor-associated macrophages are involved in tumor progression in papillary renal cell carcinoma. *Virchows Archiv.* 464: 191-196.
21. Klatter T, Rao PN, de Martino M, LaRochelle J, Shuch B, et al. (2009) Cytogenetic profile predicts prognosis of patients with clear cell renal cell carcinoma. *J Clin Oncol.* 27: 746-753.
22. Malouf GG, Camparo P, Oudard S, Schleiermacher G, Theodore C, et al. (2010) Targeted agents in metastatic Xp11 translocation/TFE3 gene fusion renal cell carcinoma (RCC): a report from the Juvenile RCC Network. *Ann Oncol.* 21: 1834-1838.
23. Argani P, Reuter V, Zhang L, Sung YS, Ning Y et al. (2016) TFEB-amplified Renal Cell Carcinomas: An Aggressive Molecular Subset Demonstrating Variable Melanocytic Marker Expression and Morphologic Heterogeneity. *Am J Surg Pathol.* 40: 1484-1495.